SIRT1 deacetylates RORγt and enhances Th17 cell generation

Hyung W. Lim,[1,3] Seung Goo Kang,[6] Jae Kyu Ryu,[2] Birgit Schilling,[7] Mingjian Fei,[1,3] Intelly S. Lee,[1,3] Amanuel Kehasse,[7] Kotaro Shirakawa,[1,3] Masaru Yokoyama,[8] Martina Schnölzer,[9] Herbert G. Kasler,[1,3] Hye-Sook Kwon,[1,3] Bradford W. Gibson,[5,7] Hironori Sato,[8] Katerina Akassoglou,[2,4] Changchun Xiao,[6] Dan R. Littman,[10,11] Melanie Ott,[1,3] and Eric Verdin[1,3]

[1]Gladstone Institute of Virology and Immunology, [2]Gladstone Institute of Neurological Disease, [3] School of Medecine, [4]Department of Neurology, [5]Department of Pharmaceutical Chemistry, University of California, San Francisco, San Francisco, CA 94158
[6]Department of Immunology and Microbial Science, The Scripps Research Institute, La Jolla, CA 92037
[7]Buck Institute for Research on Aging, Novato, CA 94945
[8]Laboratory of Viral Genomics, Pathogen Genomics Center, National Institute of Infectious Diseases, Tokyo 208-0011, Japan
[9]German Cancer Research Center, 69120 Heidelberg, Germany
[10]Molecular Pathogenesis Program, The Kimmel Center for Biology and Medicine of the Skirball Institute, [11]The Howard Hughes Medical Institute, New York University School of Medicine, New York, NY 10016

The balance of effector and regulatory T cell function, dependent on multiple signals and epigenetic regulators, is critical to immune self-tolerance. Dysregulation of T helper 17 (Th17) effector cells is associated with multiple autoimmune diseases, including multiple sclerosis. Here, we report that Sirtuin 1 (SIRT1), a protein deacetylase previously reported to have an antiinflammatory function, in fact promotes autoimmunity by deacetylating RORγt, the signature transcription factor of Th17 cells. SIRT1 increases RORγt transcriptional activity, enhancing Th17 cell generation and function. Both T cell–specific Sirt1 deletion and treatment with pharmacologic SIRT1 inhibitors suppress Th17 differentiation and are protective in a mouse model of multiple sclerosis. Moreover, analysis of infiltrating cell populations during disease induction in mixed hematopoietic chimeras shows a marked bias against Sirt1-deficient Th17 cells. These findings reveal an unexpected proinflammatory role of SIRT1 and, importantly, support the possible therapeutic use of SIRT1 inhibitors against autoimmunity.

CORRESPONDENCE
Eric Verdin:
everdin@gladstone.ucsf.edu
OR
melanie.ott@gladstone.ucsf.edu

Abbreviations used: EAE, experimental autoimmune encephalomyelitis; Foxp3, forkhead box P3; IP, immunoprecipitation; MRM-HR, high-resolution multiple reaction monitoring; MS, multiple sclerosis; RORγt, RAR-related orphan receptor γ-t; SIRT1, silent mating type information regulation 2 homolog-1.

After encountering their cognate antigens, T cells can differentiate into either immunosuppressive regulatory (T reg) or proinflammatory or cytotoxic effector (T eff) cell types, in response to specific cytokine signals that are coupled to epigenetic regulators (Yamane and Paul, 2012). Maintaining the appropriate balance between T reg and T eff cell function is critical to the maintenance of immune self-tolerance, and aberrant function of T helper 17 (Th17) effector cells has been implicated in the onset and pathogenesis of multiple autoimmune diseases, including multiple sclerosis (Kebir et al., 2007). In the affected tissues, Th17 cell differentiation is dependent on a signature transcription factor, RAR-related orphan receptor γ-t (RORγt), which is regulated by TCR and cytokine signals (Ivanov et al., 2006). The sirtuins are NAD^+-dependent protein deacetylases that play critical roles in transcriptional regulation, cell cycling, replicative senescence, inflammation, and metabolism. In mammals, SIRT1 in particular acts as an epigenetic regulator that modulates the activity of several transcription factors important for immune function (Kwon et al., 2008; Zhang et al., 2009). While initial studies on globally Sirt1-deficient mice suggested that Sirt1 has a primarily antiinflammatory function (Zhang et al., 2009; Gao et al., 2012), more recent work focusing on T cells has identified an important proinflammatory action as a negative regulator of T reg cell function, via deacetylation of Foxp3, the signature transcription factor of T reg cells (van Loosdregt et al., 2010; Beier et al., 2011; Kwon et al., 2012). However, the function of

The Rockefeller University Press $30.00
J. Exp. Med. 2015 Vol. 212 No. 5 607–617
www.jem.org/cgi/doi/10.1084/jem.20132378

The Journal of Experimental Medicine

SIRT1 in T eff cell function is still poorly understood. Here, we provide evidence that SIRT1 positively regulates the function of Th17 cells by modulating the activity of RORγt. In vivo, Sirt1 deficiency results in impaired production of proinflammatory Th17 cells and reduced susceptibility to Th17 cell–mediated autoimmune disease. These observations suggest that pharmacologic inhibition of SIRT1 may be a valuable strategy in treating conditions driven by Th17 cells, such as multiple sclerosis.

RESULTS AND DISCUSSION

SIRT1 promotes Th17 differentiation

To gain insight into the function of SIRT1 in T eff cells, we examined its expression level in different T cell subsets. We first confirmed previously reported results that SIRT1 is expressed at high levels in thymocytes and much less so in naive T cells (Fig. 1 A; Gao et al., 2012). Stimulation of naive T cells with αCD3/αCD28 antibodies alone or with additional factors that mediate effector cell differentiation increased SIRT1 expression approximately three-fold for Th0, Th1, and Th2 conditions and approximately fourfold for Th17 conditions, with no significant change during T reg cell induction (Fig. 1 A). The high expression of SIRT1 under Th17 conditions, together with previous findings that SIRT1 negatively regulates the development of T reg cell (van Loosdregt et al., 2010; Beier et al., 2011; Kwon et al., 2012), suggested that SIRT1 might play a unique role in Th17 development.

To test this possibility, we examined the effect of nicotinamide, a sirtuin inhibitor, during ex vivo Th17 induction. We observed a dose-dependent suppression of IL-17A and IL-17F production in response to nicotinamide (Fig. 1 B, left). Importantly, the inhibitory effect of nicotinamide was observed over a range of TGF-β concentrations (Fig. 1 B, right). Under the same conditions, nicotinamide dose-dependently enhanced the production of TNF, IL-2, and Foxp3, demonstrating the specificity of suppression of IL-17 production (Fig. 1 B). Th17 differentiation was also suppressed when cells were treated with Ex-527, a specific SIRT1 inhibitor (Fig. 1 C). Under Th17 cell differentiation conditions, cytokine genes associated with Th17 cell differentiation were down-regulated by nicotinamide treatment, whereas the expression of the *sirt1-7* genes was unchanged, suggesting that SIRT1 inhibitor treatment specifically affected Th17 differentiation process (Fig. 1 D).

To further assess the role of SIRT1, we crossed mice carrying a loxp site-flanked Sirt1 allele ($Sirt1^{fl/fl}$) with mice expressing Cre under the control of the RORγt promoter (RORγt-Cre), leading to the specific deletion of SIRT1 in RORγt-expressing cells ($Sirt1^{-/-}$). We observed that CD4 T cells lacking SIRT1 did not affect RORγt protein expression (Fig. 1 E), but showed reduced Th17 cell differentiation ex vivo compared with littermate controls over a broad range of TGF-β concentrations (Fig. 1 F). Importantly, treatment with Ex-527 suppressed Th17 cell differentiation in WT CD4 T cells but had no effect on T cells lacking SIRT1 (Fig. 1 G), demonstrating the specificity of the Ex-527 effect to SIRT1.

To test the relative fitness of WT CD4 T cell and $Sirt1^{-/-}$ CD4 T cells to differentiate in vivo into Th17 or T reg cell cells, we generated WT: $Sirt1^{-/-}$ mixed hematopoietic bone marrow chimeras using a 1:1 ratio of WT and $Sirt1^{-/-}$ donor cells. Strain-specific allotypic markers (CD45.2 for $Sirt1^{-/-}$ and CD45.1 for WT), were used to follow the origin and relative contribution of cells derived from each donor strain. Splenocytes isolated from reconstituted chimeras showed a strong bias against Th17 differentiation in cells lacking SIRT1 relative to WT cells (Fig. 1 H). The opposite phenotype was observed for T reg cell with more cells originating from the $Sirt1^{-/-}$ donor than from the WT donor (Fig. 1 H). In contrast, the respective contributions of both donors to the IL-2 producing cell population were not significantly different from each other. Similarly, small intestinal lamina propria-infiltrating lymphocytes from reconstituted chimeras showed a bias against Th17 and toward T reg cell differentiation in cells lacking SIRT1 relative to WT cells (unpublished data). Overall, the ratio of Th17/T reg cells was ∼5-fold higher for the WT than for the $Sirt1^{-/-}$ population, confirming a critical, cell autonomous role for SIRT1 in controlling the Th17/T reg cell ratio in vivo (Fig. 1 H).

SIRT1 physically interacts with RORγt

Because RORγt is the major lineage-specific transcription factor for Th17 differentiation and RORγt protein induction was not affected by SIRT1, we hypothesized that SIRT1 might regulate RORγt activity. In support of this model, we found that RORγt interacts with both WT SIRT1 and SIRT1-H363Y, a catalytically inactive mutant, in transiently transfected 293T cells (Fig. 2 A). Similarly, endogenous RORγt could be co-immunoprecipitated with endogenous SIRT1 in both thymocytes and Th17 cells (Fig. 2 B). Immunoprecipitation experiments using deletion mutants of RORγt showed that SIRT1 binds to the C-terminal part of RORγt (aa 99–495). The ligand-binding domain (aa 304–495) of RORγt was sufficient for SIRT1 binding, whereas the DNA binding domain of RORγt (aa 1–99) did not bind (Fig. 2 C).

Next, we tested whether RORγt is acetylated. Co-transfection of expression vectors for the lysine acetyltransferase p300 (KAT3B) with RORγt led to its robust acetylation in 293T cells (Fig. 2 D). No significant change in RORγt acetylation was observed when four other lysine acetyltransferases, CBP (KAT3A), PCAF (KAT2B), GCN5 (KAT2A), or TIP60 (KAT5), were coexpressed with RORγt (Fig. 2 D). Importantly, coexpression of WT SIRT1, but not a catalytically inactive SIRT1 (SIRT1-H363Y), effectively deacetylated RORγt (Fig. 2 E). Furthermore, nicotinamide or Ex-527 treatment rescued SIRT1-mediated RORγt deacetylation (Fig. 2 F).

SIRT1 deacetylates three lysine residues in the RORγt DNA binding domain

Mass spectrometric analysis of immunoprecipitated RORγt from transiently transfected 293T cells robustly identified several lysine residues in RORγt that were acetylated by

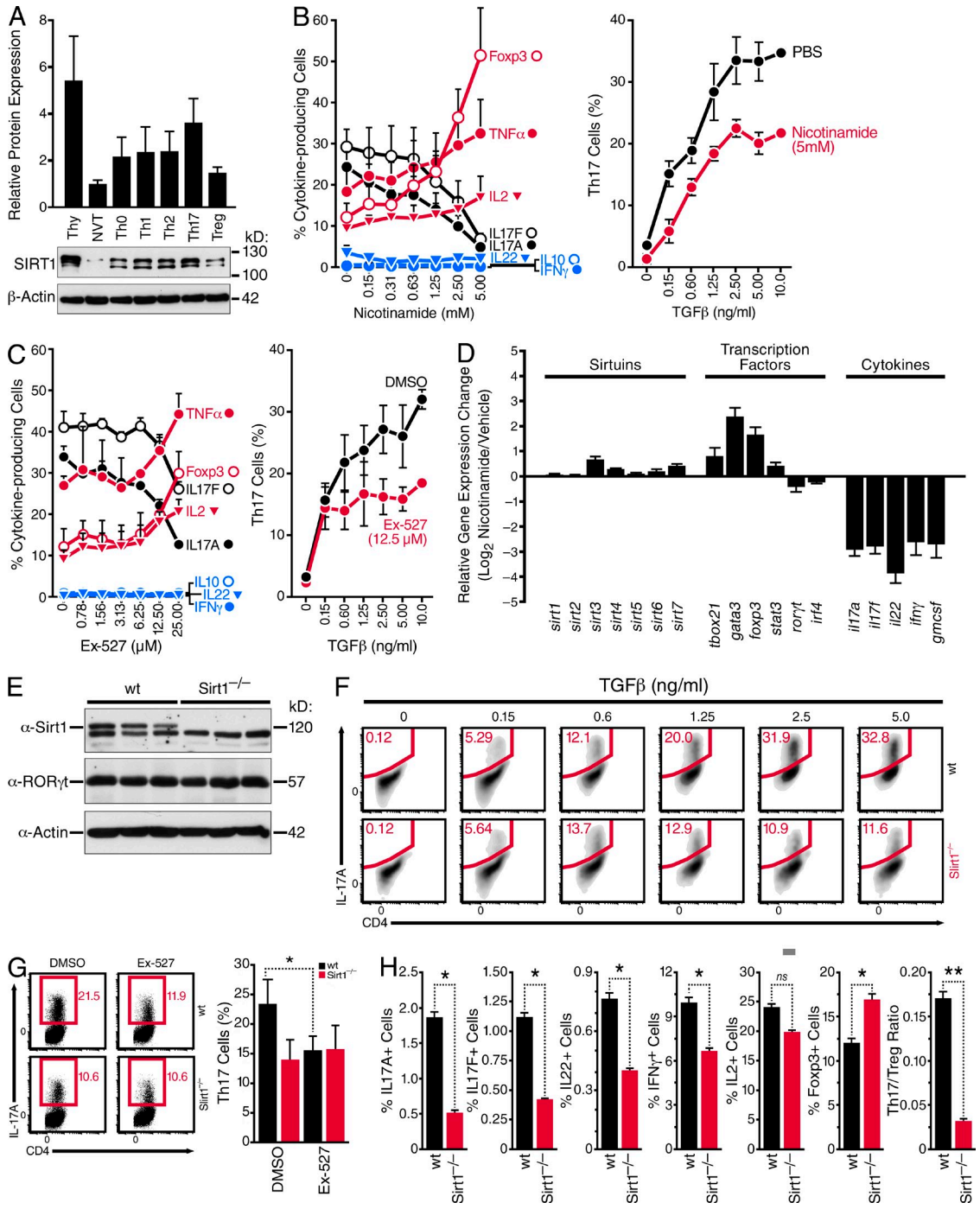

Figure 1. SIRT1 promotes Th17 differentiation ex vivo and in vivo. (A) Freshly isolated naive T (NVT) cells from C57BL/6 (B6) mice were differentiated ex vivo into various effector T cells as indicated (Materials and methods). Thy, thymocytes. SIRT1 expression was determined by Western blot using β-actin as an internal control. (B and C) Naive CD4 T cells from WT B6 mice were differentiated into Th17 cells in the presence of various amounts of nicotinamide (B) or Ex-527 (C). (D) Relative gene expression between 1.25 mM nicotinamide treated and untreated cells was determined for the indicated genes by qPCR. (E) Th17 cell protein lysates from WT and Sirt1$^{-/-}$ mice were subjected to Western blot analysis to visualize SIRT1 knock-out efficiency. (F) Naive T cells from WT and Sirt1$^{-/-}$ mice were differentiated into Th17 cells with the indicated amounts of TGF-β1. (G) Naive CD4 T cells from WT and Sirt1$^{-/-}$ mice were differentiated into Th17 cells with 2.5 ng/ml of TGFβ1 in the presence of 12.5 μM of Ex-527. (H) 12 wk after engraftment, total splenocytes from CD45.1 WT/CD45.2 Sirt1$^{-/-}$ (1:1) mixed hematopoietic chimeras were stained with antibodies against IL-17A, IL-17F, IL-22, IFN-γ, IL-2, and Foxp3, together with CD4, CD45.1, and CD45.2. Percentage of cytokine-expressing cells was measured by flow cytometry 3–6 d after differentiation. Error bars represent (±SEM) for data from three (A, B [right], C [right], D, and G), four (B [left], C [left]), or five (H, total 14 mice/condition) independent experiments. Also, representative data from one (E), two (F), and three (A and G) independent experiments is shown. Significance values are based on a two-tailed Student's *t* test. *, $P < 0.05$; **, $P < 0.01$.

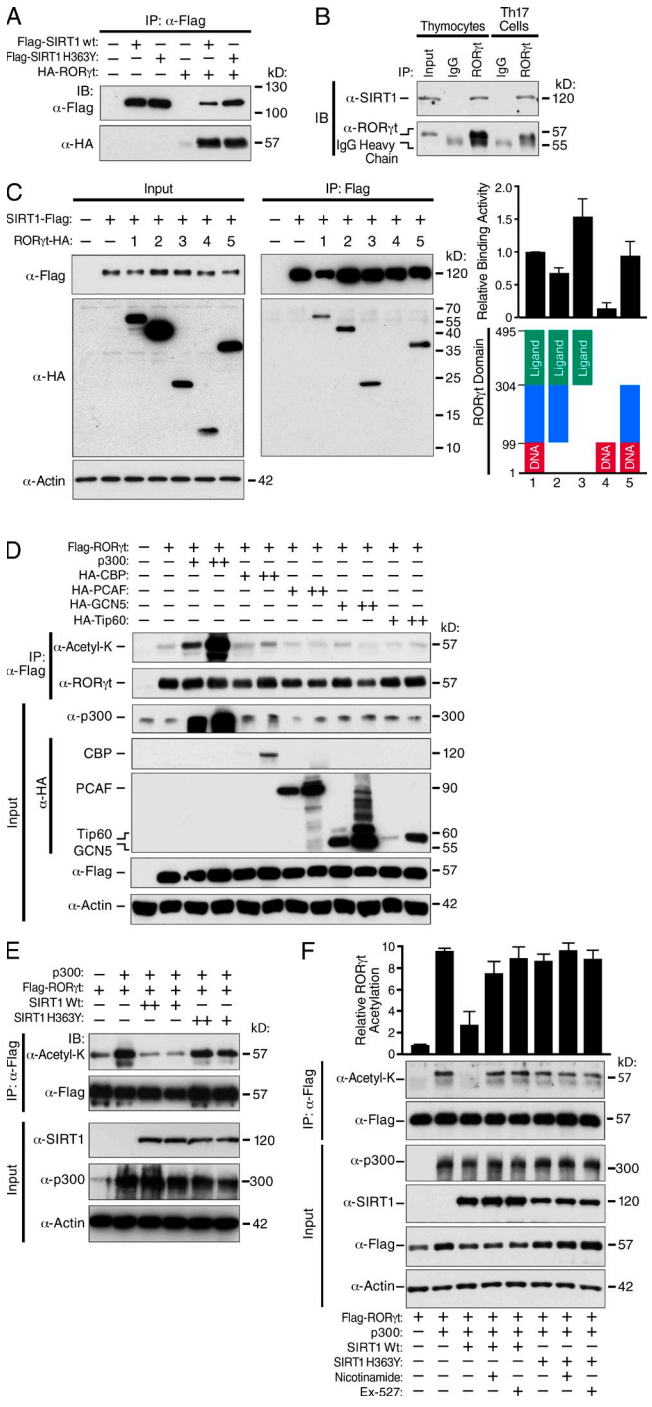

Figure 2. SIRT1 interacts with RORγt. (A) Flag-tagged WT or H363Y mutant SIRT1 was immunoprecipitated from transfected 293T cells and probed as indicated. (B) RORγt was immunoprecipitated from thymocytes and Th17 cells, and probed with antibody against SIRT1. (C) Immunoprecipitation using lysates of 293T cells co-transfected with constructs encoding SIRT1 and various deletion mutants of RORγt. Relative binding was calculated by normalizing the ratio of immunoprecipitated RORγt/SIRT1 to the ratio of input RORγt/SIRT1. (D) Acetylation of Flag-tagged RORγt immunoprecipitated from 293T cells transfected with various acetyltransferases and Flag-RORγt. (E and F) Acetylation of Flag-RORγt co-transfected with p300 and WT or H363Y mutant SIRT1, in the absence (E) or in the presence (F) of nicotinamide and Ex-527. Equal amounts of Flag-RORγt were loaded (D–F). Representative data are shown from four (A), three (B and E), and two (D) independent experiments, and combined data are shown from three (C and F) independent experiments with error bars representing ±SEM.

p300, with the most prominent acetylation sites at K69, K81, K99, and K112. In the presence of SIRT1, three of these residues (K69, K81, and K99) became deacetylated (Fig. 3 A). Because these three residues are located in the DNA-binding domain of RORγt, we modeled the interaction of RORγt with DNA using the x-ray crystal structure of a closely related transcription factor (Retinoid X Receptor or RXR, PDB code: 2NLL; Rastinejad et al., 1995; Zhao et al., 2000) bound to DNA. This analysis revealed that the side chains of the three SIRT1 regulated lysine residues, K69, K81 (particularly), and K99 are predicted to be positioned near the DNA. In addition, K69 is predicted to be in the immediate vicinity of the zinc atom in the zinc finger of RORγt (Fig. 3 B). Additional RORγt acetylation sites with corresponding MS/MS spectra and detailed information are presented in Fig. S1 and Table S1. Our overall RORγt sequence coverage was 81.2% (Table S1).

Although acetylation of RORγt was observed in this overexpression system, we had not yet assessed whether RORγt is actually acetylated in primary cells. To investigate this important question, we examined the acetylation of endogenous RORγt from both thymocytes and Th17 cells. Immunoprecipitation of the endogenous protein, followed by blotting with antibodies for acetyllysine, revealed that RORγt is acetylated in both cell types and, moreover, that RORγt from Sirt1$^{-/-}$ cells was hyperacetylated relative to that from WT cells (Fig. 3, C and D). Mass spectrometric analysis of the immunoprecipitated RORγt from thymocytes confirmed acetylation of 7 lysine residues in RORγt, including K99 acetylation (Fig. 3 E, Table S2). Next, we quantified the acetylation level of lysine residues in RORγt from both thymocytes and Th17 cells, using a high-resolution multiple reaction monitoring (MRM-HR) assay targeting all the acetylated peptides previously observed in 293T cells, as well as several unmodified peptides used to control for differences in total protein. Extracted ion chromatograms monitored by MRM-HR revealed that ~1.8-fold less protein was present for control peptides in Sirt1$^{-/-}$ Th17 cells (Fig. 3 F, top), but ~2-fold increased acetylation was observed for K99 in Th17 cells lacking SIRT1 relative to WT cells (Fig. 3 F, bottom). Indeed, the K81, K87/88, and K99 residues in RORγt were all hyperacetylated in Sirt1$^{-/-}$ Th17 cells (Fig. 3 G and Fig. S2) and K69, K81, K87/88, and K99 residues in RORγt were hyperacetylated in thymocytes (Fig. 3 H and Fig. S3). We noticed that although the acetylation level of K87/88 residues was low in WT, these sites were found to be hyperacetylated in both thymocytes and Th17 cells lacking SIRT1 relative to WT, suggesting a key role for SIRT1 in deacetylating these positions. Interestingly, we also found that the T113 position in RORγt was phosphorylated, and this was

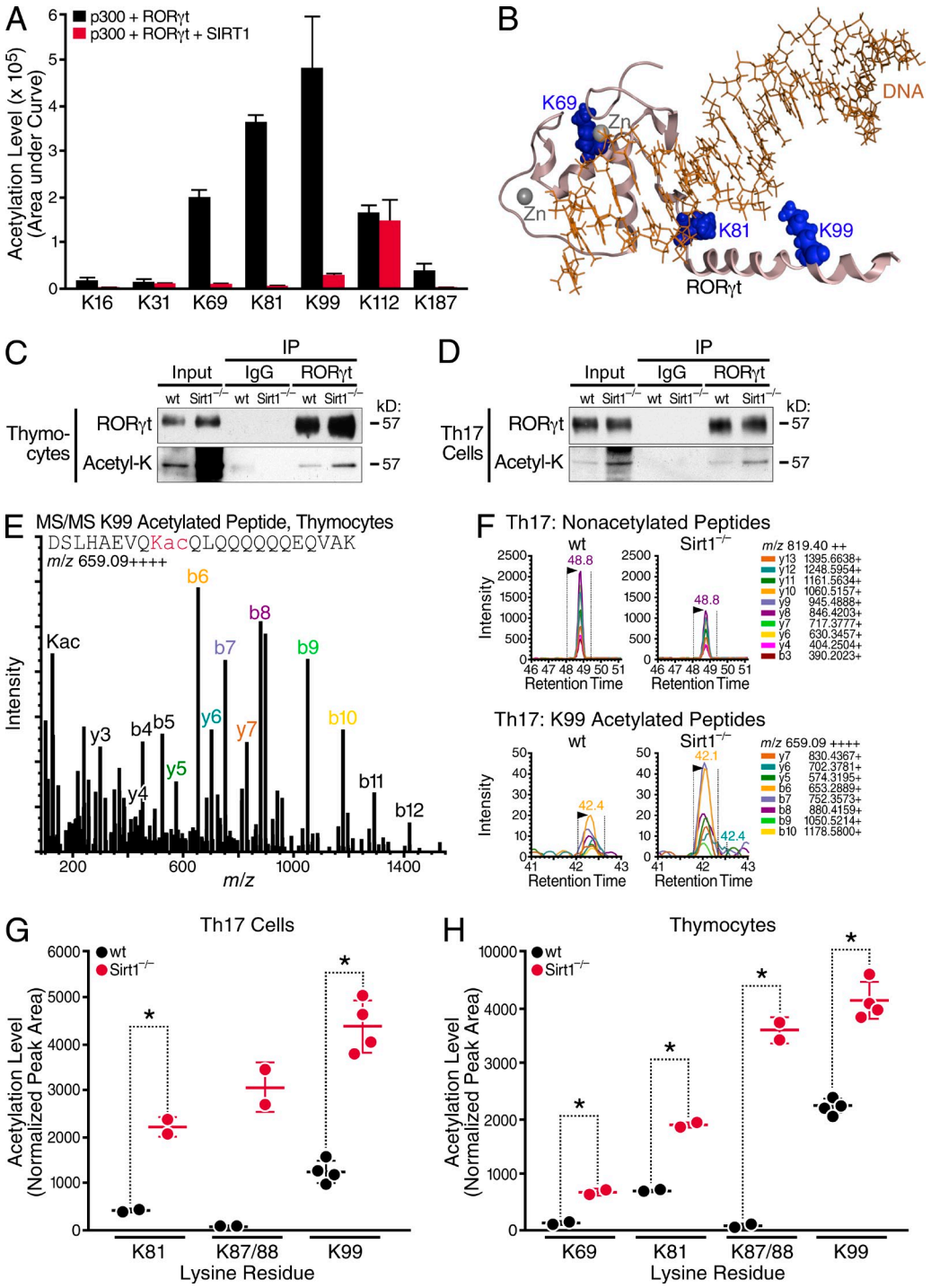

Figure 3. SIRT1 deacetylates RORγt. (A) Flag-RORγt immunoprecipitated from 293T cells expressing p300 and RORγt (black bars), or p300, RORγt, and SIRT1 (red bars) was analyzed by mass spectrometry, identifying the indicated acetylated lysines and changes in their respective MS1 precursor ion abundances. (B) Structural model of acetylated RORγt with DNA. The N-terminal DNA-binding domain of RORγt with DNA is shown. The blue globules indicate side chains of the K69, K81, and K99 residues that are strongly acetylated by p300 and deacetylated by SIRT1. (C and D) Acetylation of endogenous RORγt immunoprecipitated from thymocytes (C) and Th17 cells (D) was determined by Western blot. (E) MS/MS spectrum of acetylated peptide containing Kac-99 from RORγt. (F) Targeted MRM-HR showing the protein level of RORγt in Th17 cells (top panel, nonacetylated peptide ELFSTDVESPEGLSK, *m/z* at 819.40^{2+}), as well as potential RORγt acetylation level changes at residue Kac-99 (bottom, acetylated peptide DSLHAEVQKacQLQQQQQQEQVAK, *m/z* at 659.09^{++++}). (G and H) Acetylated tryptic peptides were monitored by MRM-HR, in technical duplicates between WT and Sirt1$^{-/-}$ pooled mice (10 mice per each genotype), to quantify differences in RORγt acetylation levels in Th17 cells (G) and in thymocytes (H). Peptides assayed for each acetylated lysine were as follows: Kac-69, LQKacCLALGM^{ox}SR, *m/z* at 667.85^{2+} (thymocytes only); Kac-81, DAVKacFGR, *m/z* at 417.73^{2+};

not affected by SIRT1 in either cell type (Figs. S2 and S3). All quantitative results and the detailed MRM-HR assays are provided in Table S2. These observations strongly support the idea that SIRT1 deacetylates RORγt in its DNA binding domain. We also noticed that the total protein level of RORγt in Th17 cells from Sirt1$^{-/-}$ mice was lower than that from WT mice (Fig. 3, D and F). However, based on multiple trials for Fig. 3 D, Western blot data using three mice per genotype (Fig. 1 D), and intracellular staining of RORγt at different time points during Th17 cell differentiation (unpublished data), we conclude that SIRT1 deficiency does not appreciably alter RORγt expression in Th17 cells.

Acetylation of RORγt modulates IL-17A and IL-2 transcription

RORγt exerts opposing transcriptional effects on two key genes in Th17 cells: it activates the IL-17 promoter and represses the IL-2 promoter. Both activities of RORγt are critical for Th17 cells since IL-2 is a negative regulator of Th17 cell differentiation (He et al., 1998; Laurence et al., 2007; Littman et al., 1999; Quintana et al., 2012; Zhang et al., 2008). We therefore examined the effect of mutating the RORγt acetylation sites we identified on its activities at both of these key target promoters. We first transfected two constructs containing the IL-17 or IL-2 promoter driving firefly luciferase with an expression vector for WT RORγt, and confirmed that RORγt both strongly activates the IL-17 promoter (up to 12 fold) and represses the IL-2 promoter (maximum sixfold repression) in a dose-dependent manner (Fig. 4 A). Next, we tested the effect of mutating the acetylated sites of RORγt on its activating and repressive activities. We transfected expression vectors for RORγt WT, single, double, or triple K>Q and K>R mutations into Jurkat cells together with the IL-17 or IL-2 reporter constructs. We observed that the K69, 81, 99Q (3K>Q) mutant, mimicking a constitutively acetylated form of RORγt, induced substantially weaker IL-17 transcription than WT RORγt (Fig. 4 B). In agreement with these data, the same mutant (3K>Q) lost its ability to suppress the IL-2 promoter (Fig. 4 C). Importantly, the acetylation-resistant 3K>R mutant behaved similarly to WT RORγt, suggesting that RORγt is not significantly acetylated in Jurkat cells. As Jurkat cells express high levels of SIRT1 (unpublished data), and would likely deacetylate any overexpressed RORγt, these results support our hypothesis that deacetylated RORγt is the most effective form at promoting IL-17 transcription and suppressing IL-2 transcription. We also confirmed this observation in primary CD4 T cells. When naive T cells were transduced with retrovirus encoding 3K>Q mutant RORγt during their initial activation, they failed to differentiate into Th17 cells under either Th0 or Th17 polarizing conditions (Fig. 4 D). In contrast, transduction with the 3K>R RORγt mutant produced a similar effect to WT RORγt (Fig. 4 D). Because Aiolos is also known to regulate IL-2 production in Th17 cells (Quintana et al., 2012), we examined its effect on IL-2 transcriptional activity in the presence of RORγt. In agreement with previous findings, Aiolos itself strongly suppressed IL-2 promoter activity and together with RORγt, it further repressed IL-2 promoter activity (unpublished data).

Finally, to investigate the significance of SIRT1 deacetylation of RORγt in the suppression of IL-2 transcription, we tested whether addition of neutralizing IL-2 antibody could rescue IL-17 production in Sirt1$^{-/-}$ T cells. We observed a partial rescue of Th17 cell differentiation in Sirt1$^{-/-}$ T cells (Fig. 4 E). Indeed, IL-2 production was sevenfold higher for Sirt1$^{-/-}$ T cells than WT T cells under Th17 differentiation conditions (Fig. 4 F), suggesting that the regulation of IL-2 via RORγt acetylation contributes significantly to the effect of SIRT1 on Th17 cell differentiation. These data indicate that deacetylation of RORγt by SIRT1 at unique lysine residues in its DNA-binding domain is important for optimal transcriptional activity, and also elucidate one important mechanism through which loss or inhibition of SIRT1 function inhibits Th17 cell generation.

Inhibition of SIRT1 activity protects mice from EAE

We next evaluated whether interfering with SIRT1 function in T cells could ameliorate disease progression in a Th17 cell–dependent animal model of autoimmunity. Experimental autoimmune encephalomyelitis (EAE) is a mouse model for human multiple sclerosis (MS), which develops in response to immunization with a myelin oligodendrocyte glycoprotein (MOG)-derived peptide in complete Freund's adjuvant. Sirt1$^{-/-}$ mice were significantly protected from EAE compared with littermate controls (Fig. 5 A). Treatment with Ex-527 (10 mg/kg, subcutaneous injection) in WT mice was even more effective at ameliorating EAE, not only lessening ultimate disease severity but also significantly delaying its onset (Fig. 5 B). Spinal cords from Ex-527 treated mice exhibited markedly less lymphocytic infiltration and demyelination compared with vehicle-treated controls (Fig. 5, C–E).

Finally, we evaluated the effect of SIRT1 regulation of RORγt in EAE in WT/Sirt1$^{-/-}$ mixed hematopoietic chimeras. During a late stage of disease after induction, significantly fewer infiltrating Sirt1$^{-/-}$ CD4 T cells than WT CD4 T cells were recovered from affected spinal cords, despite their ∼3 fold higher prevalence in spleen and lymph nodes (Fig. 5 F). Furthermore, whereas ∼30% of the infiltrating WT CD4 T cells produced IL-17A, only ∼9% of Sirt1$^{-/-}$ derived infiltrating CD4 T cells contributed to the Th17 cell pool (Fig. 5). Conversely, Foxp3^{+} T reg cells derived from Sirt1$^{-/-}$ donors were twice as abundant as those derived from WT donors in the spinal cord (Fig. 5 G). The cytokine profile of T reg cells

Kac-87/88, MSKacKacQR, *m/z* at 431.23^{2+}; and Kac-99, DSLHAEVQKacQLQQQQQQEQVAK, *m/z* at 878.45^{+++} and 659.09^{++++}. Peak areas were normalized to account for RORγt protein level changes. Significance was assessed using a two-tailed Student's *t* test ($P < 0.05$). Combined data from two (A) independent experiments or representative data from two (D; 3 mice/genotype) and three (C; 10 mice/genotype) independent experiments are shown. *, $P < 0.05$.

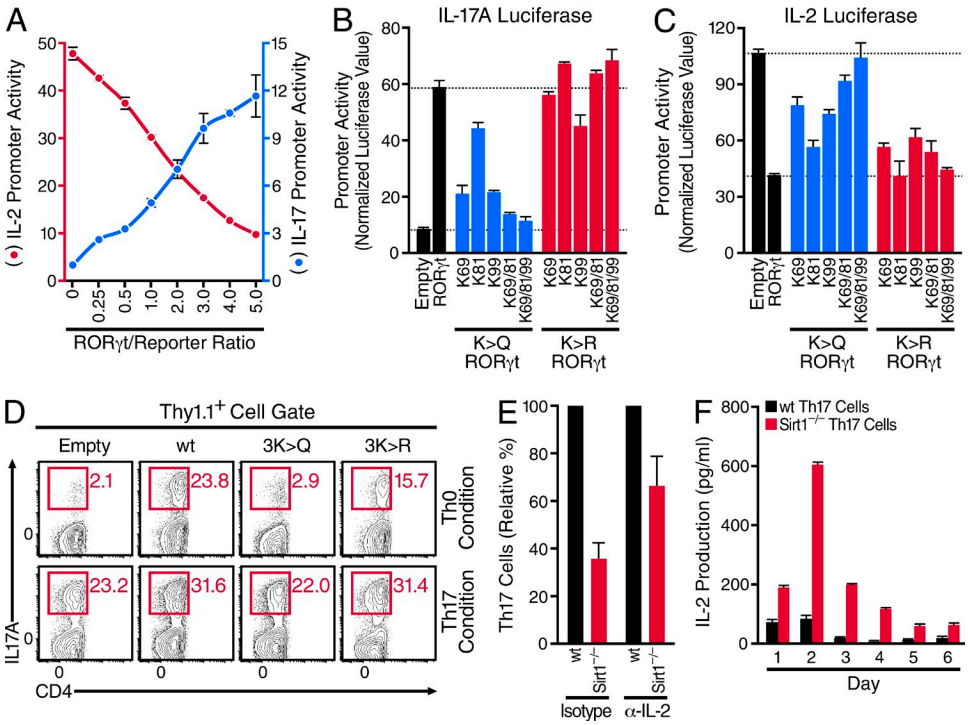

Figure 4. SIRT1 modulates IL-17A and IL-2 transcriptional activity via deacetylation of RORγt. (A) Jurkat cells were transiently transfected with RORγt, a TK-driven *Renilla* luciferase vector, and either IL-17A (blue symbols) or IL-2 (red symbols) promoter-driven firefly luciferase reporter constructs. (B and C) Jurkat cells were transiently transfected with TK *Renilla* luciferase and either an IL-17A firefly reporter construct (B) or an IL-2 firefly reporter construct (C), as well as WT, single, double, or triple RORγt mutants. Firefly luciferase values were normalized to *Renilla* luciferase values. Error bars represent ±absolute value of differences between duplicate samples. (D) CD4 T cells from B6 mice were infected with retrovirus carrying either Thy1.1 alone or Thy1.1 together with WT or mutant RORγt as indicated, and further differentiated under Th0 (top) or Th17 (bottom) conditions. IL-17A secretion was measured. (E) Naive CD4 T cells from WT and Sirt1$^{-/-}$ mice were differentiated into Th17 cells in the presence of either isotype control antibody or IL-2 neutralizing antibody. The relative percentage of Th17 cells was examined. (F) Secreted IL-2 from WT and Sirt1$^{-/-}$ cells cultured under Th17 differentiation conditions was measured by ELISA. Error bars represent ±SEM from triplicate samples. Representative data from two (A and F), or three (B–D) independent experiments or combined data from four (E) independent experiments are shown.

derived from Sirt1$^{-/-}$ mice was not statistically different from that of T reg cells derived from WT mice (Fig. 5 H), suggesting that Sirt1$^{-/-}$ mice derived T reg cells function normally. Overall, the ratio of Th17 to T reg cells was fivefold higher for pathogenic, infiltrating WT T cells than for Sirt1$^{-/-}$ T cells (Fig. 5 G, right). Together, these data demonstrate a critical in vivo role for SIRT1 in controlling the Th17/T reg cell balance in autoimmune disease. Although we cannot rule out a contributing role for SIRT1 in RORγ^{+} innate lymphoid cells and lymphoid tissue-inducing cells, our data are strongly supportive of a model where SIRT1 activity cell-autonomously regulates the Th17/T reg cell balance both in normal homeostasis and in Th17 cell–dependent autoimmune disease.

Thus, although prior studies have suggested that SIRT1 broadly suppresses inflammation (Zhang et al., 2009), our findings demonstrate a clear proinflammatory role for SIRT1 in the context of Th17 effector cell differentiation. By deacetylating both RORγt as shown here and Foxp3 as shown previously (van Loosdregt et al., 2010; Beier et al., 2011; Kwon et al., 2012), SIRT1 enhances the activity of RORγt and reduces the activity of Foxp3, promoting Th17 cell development at the expense of regulatory T cells and thus establishing conditions favorable for the development of autoimmunity. Consistent with this, treatment with Ex-527, a SIRT1-specific inhibitor strongly suppressed the development of EAE in mice, suggesting that SIRT1 inhibition may represent a potent therapeutic modality for the treatment of Th17 cell–mediated autoimmune diseases in humans.

MATERIALS AND METHODS

Mice. C57BL/6 (B6) WT mice, BoyJ mice, and Sirt1$^{fl/fl}$ mice were obtained from The Jackson Laboratory. RORγt-Cre mice were generated by D.R. Littman. Mice were maintained in a specific pathogen–free facility at the J. David Gladstone Institutes (University of California, San Francisco, San Francisco, CA). All experiments were performed in accordance with animal use protocols approved by the University of California, San Francisco and Scripps Research Institutes Animal Care and Use Committees.

Cell isolation and in vitro T cell differentiation. CD4 T cells were isolated from spleen and lymph nodes by magnetic bead depletion using a CD4 T cell isolation kit (Miltenyi Biotec). Naive T cells were further isolated using naive T cell isolation kit (StemCell Technologies) or phycoerythrin (PE)-conjugated antibodies against CD25 and CD44, followed by PE magnetic bead depletion (Miltenyi Biotec). Freshly isolated naive T cells were differentiated into different T cell subsets with plate-bound αCD3 (5 μg/ml; 145-2C11) and soluble αCD28 (2 μg/ml; PV-1) in the presence of appropriate cytokines (Th0: 20 U/ml rhIL-2, 5 μg/ml

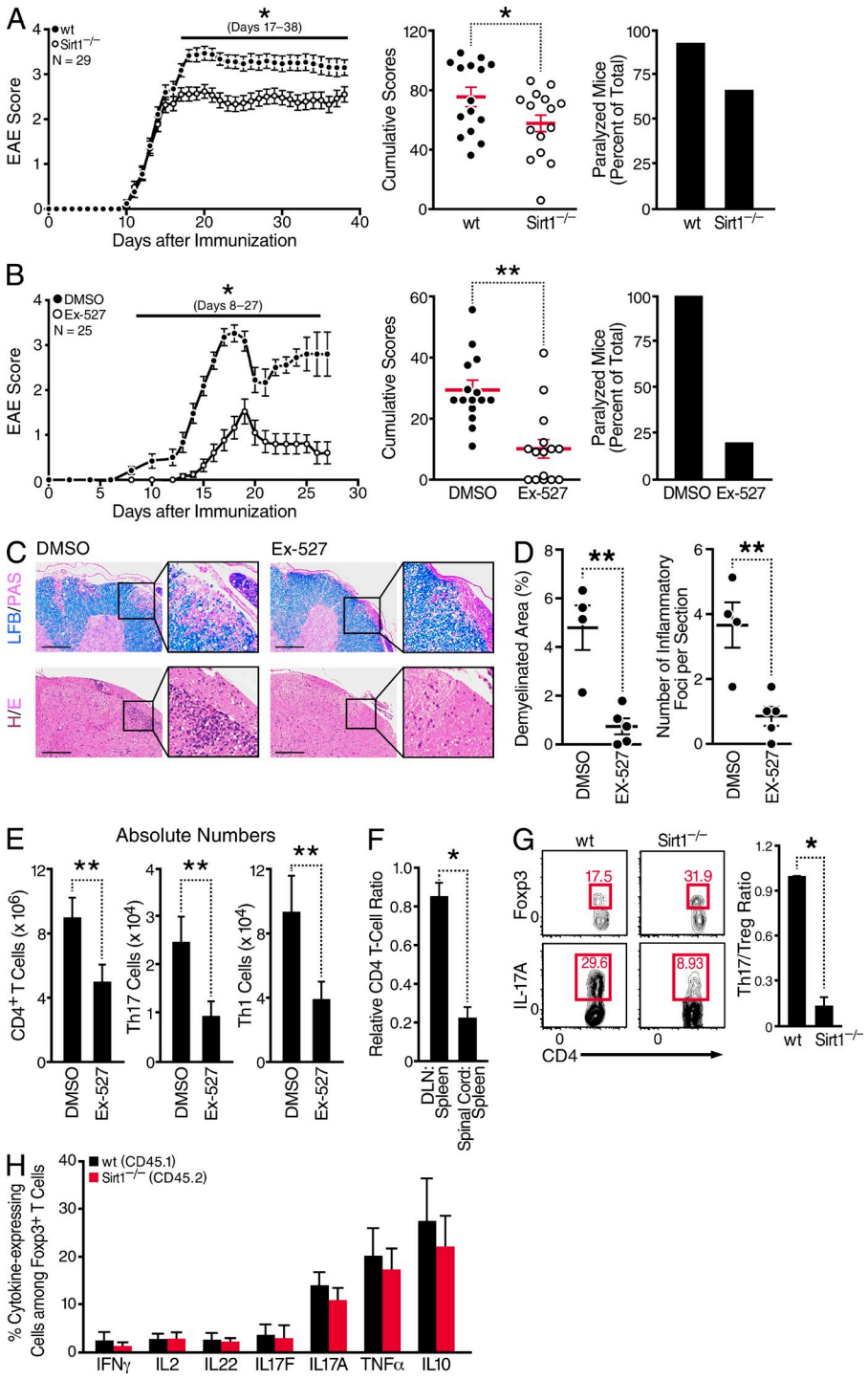

Figure 5. Deletion of SIRT1 in T cells or chemical inhibition of SIRT1 protects mice from EAE. (A) EAE clinical scores of WT and Sirt1$^{-/-}$ mice after MOG_{35-55} peptide immunization. (B) EAE clinical scores of WT mice immunized with MOG_{35-55} peptide followed by treatment with DMSO or Ex-527 at 0, 1, and 2 d after immunization. (C) Representative histological sections of spinal cords of DMSO (left) and Ex-527–treated mice (right) from (B). 28 d after immunization, panels were stained for demyelination (LFB/PAS) and lymphocytic infiltration (H&E). Bars, 200 µm. (D) Quantification of demyelination (left) and number of inflammatory foci (right) for DMSO and Ex-527–treated mice. (E) Quantification of spinal cord infiltrated T cell subsets from DMSO and Ex-527 treated mice. (F–H) WT: Sirt1$^{-/-}$ mixed hematopoietic chimeras were immunized with MOG_{35-55} peptide. Relative CD4 T cell ratio of Sirt1$^{-/-}$ to WT was calculated (F), spinal cords were analyzed for Foxp3$^+$ and IL-17A$^+$ CD4 T cells (G), or Foxp3$^+$ CD4 T cells producing the indicated cytokines (H) were examined, when the mice reached an EAE clinical score of 3. Error bars represent mean ±SEM. Combined data from two (A; 15 mice/each experiment) and three (B; 5–10 mice/each experiment and F, total 10 mice) independent experiments are shown. Representative or combined data from four (C and D), five (E and H), and seven (G, left) mice are shown. *, $P < 0.05$, **, $P < 0.01$.

αIFN-γ antibody, and 5 µg/ml αIL-4 antibody; Th1: 10 ng/ml rmIL-12 and 5 µg/ml αIL-4 antibody; Th2: 10ng/ml rmIL-4 and 5 µg/ml αIFN-γ antibody; Th17: 20 ng/ml rmIL-6, 2.5 ng/ml rhTGFβ1, 5 µg/ml αIFN-γ antibody, and 5 µg/ml αIL-4 antibody;T reg cells: 20 U/ml rhIL-2 and 5 ng/ml rhTGFβ1). All cytokines were purchased from PeproTech unless otherwise stated. For some Th17 differentiation experiments, TGF-β1, Nicotinamide (Sigma-Aldrich), or Ex-527 (Tocris) was added as indicated in the corresponding figures.

Retrovirus infection. To obtain recombinant virus, 10 µg retrovirus encoding Thy1.1 and WT/mutant RORγt or control virus encoding Thy1.1 alone was transfected into phoenix-eco cells. Supernatants were collected 48 h after transfection and were filtered through a 0.45-µm membrane. Naive CD4 T cells were activated for 24 h with αCD3 and αCD28, were infected twice with retroviral supernatant in the presence of polybrene (6 µg/ml) by spin-inoculation at 2,000 rpm for 90 min and were further activated for 3 d with αCD3 and αCD28, in either Th0 or Th17 differentiation condition.

EAE induction. EAE was induced in 10-wk-old female B6 WT and Sirt1$^{-/-}$ mice by subcutaneous immunization with MOG_{35-55} peptide in complete Freund's adjuvant, followed by pertussis toxin injection on days

0 and 2 of the immunization intraperitoneally (Davalos et al., 2012). To examine Ex-527 effect on EAE induction, either DMSO or Ex-527 (10 mg/kg) were subcutaneously injected on day 0, 1, and 2 after EAE induction. Mice were scored daily as follows: 0, no symptoms; 1, loss of tail tone; 2, ataxia; 3, hind limb paralysis; 4, hind limb and fore limb paralysis; 5, moribund. Experiments were performed in a blinded manner to the genotypes in two separate mouse cohorts. Data are represented as the mean clinical score with error bars (±SEM), and the Mann-Whitney *U* test was used for statistical analysis using PRISM software.

Histopathology. Histopathological analysis was performed on paraffin sections. Sections were stained with hematoxylin/eosin or luxol fast blue/periodic acid-Schiff. Images were acquired with an Axioplan II epifluorescence microscope (Carl Zeiss, Inc.) equipped with dry Plan-Neofluar objectives (10 × 0.3 NA, 20 × 0.5 NA, or 40 × 0.75 NA). Number of inflammatory foci and demyelinated area were quantified using ImageJ (National Institutes of Health) by a blinded observer as described previously (Adams et al., 2007).

Transient transfection and immunoprecipitation. 293T cells were transfected at 70–80% confluency with vectors for Flag-RORγt, HA-SIRT1, and myc-p300 (pcDNA3.1) in a 1:2:4 ratio by either calcium phosphate or Lipofectamine 2000 (Invitrogen), as indicated. Total transfected DNA for each sample was normalized by adding empty vector DNA. 6–8 h after transfection, cells were washed and media was replaced followed by treatment with TSA (400 nM) for 18 h to induce p300 hyperacetylation of RORγt. Cells were harvested in p300 lysis buffer (250 mM NaCl, 0.1% NP-40, 20 mM NaH_2PO_4, pH 7.5, 5 mM EDTA, 30 mM sodium pyrophosphate, 10 mM NaF, 5 mM nicotinamide, 400 nM TSA [Sigma-Aldrich], nicotinamide [5 mM; Sigma-Aldrich], and HALT protease/phosphatase inhibitors [Thermo Fisher Scientific]). After clarification, lysates were immunoprecipitated with α-Flag (M2) conjugated-agarose (Sigma-Aldrich), washed 5 times with lysis buffer and eluted with Flag peptide (100 μg/ml). Samples were boiled in Laemmli buffer for SDS-PAGE and Western blotting, and membranes were probed with antibodies against Flag (M2, Sigma-Aldrich) and pan-acetyllysine (9441; Cell Signaling Technology).

Endogenous RORγt immunoprecipitation. Total thymocytes and differentiated Th17 cells from WT and Sirt1$^{-/-}$ mice were treated with TSA (2 μM) for 45 min before harvest to induce basal protein acetylation. Cells were harvested in p300 lysis buffer. After clarification, lysates were immunoprecipitated with 1.5 μg of RORγt Ab (Q31-378; BD) for 16 h at 4°C, incubated with protein A agarose beads for 6 h, washed 5 times with lysis buffer. and then eluted RORγt protein from beads with nonreducing Laemmli buffer by boiling for 3 min. Samples were subjected to Western blotting, and membranes were probed with antibodies against RORγt (B2D; eBioscience), SIRT1 (1F3; Cell Signaling Technology), and pan-acetyllysine (9441; Cell Signaling Technology).

Luciferase reporter assay. Jurkat cells were transfected with a TransIT-Jurkat transfection reagent (Mirus). The cells were transfected with either IL-17 or IL-2 luciferase reporter construct plasmid (Addgene) along with plasmid encoding WT or mutant RORγt plasmid, and/or plasmid encoding Aiolos. Transfected cells were incubated 24 h, and then were either stimulated for 4 h with 10 ng/ml phorbol 12-myristate 13-acetate (PMA) and 500 nM ionomycin for IL-17 luciferase assay or stimulated for 6 h with 50 ng/ml PMA and 1 μM ionomycin for IL-2 luciferase assay. Cells were lysed and firefly and renilla luciferase activities were measured with a dual-luciferase assay system (Promega), then firefly values were normalized to TK-promoter driven renilla luciferase values. Each transfection was done in duplicate.

Bone-Marrow mixed chimera. CD45.1/CD45.2 heterozygote mice were lethally irradiated (1,100 rads) and reconstituted with 5 × 10^6 cells of a 1:1 mixture of CD45.1 WT and CD45.2 Sirt1$^{-/-}$ bone marrow cells. Eight weeks after reconstitution, spleen, lymph nodes, and small intestine were collected and the percentages of Foxp3-expressing and cytokine-producing CD4 T cells were determined by FACS. For some experiments, 8-wk after bone marrow transplantation, EAE was induced in female CD45.1/CD45.2 heterozygote recipient mice. Once the EAE score reached 3, spinal cord, spleen, and lymph nodes were collected from the mice and then Foxp3-expressing and cytokine-producing CD4 T cells were examined by FACS.

Molecular modeling of the complex of RORγt protein and DNA. The three-dimensional (3-D) model of the complex of the RORγt protein and DNA was constructed by the homology modeling using 'MOE-Align' and 'MOE-Homology' in the Molecular Operating Environment (MOE; Chemical Computing Group Inc.) by incorporating the multiple sequence alignment method (Shirakawa et al., 2008). The x-ray crystal structure of the complex of the retinoic acid receptor and thyroid hormone receptor and DNA at a resolution of 1.9 Å (PDB code: 2NLL; Rastinejad et al., 1995) was used as the modeling template, because the template assures high resolution and has more information on DNA structure. To minimize misalignments of the RORγt and template sequences, we used the multiple sequence alignment method with the 19 homologous sequences searched by MOE-Search-PDB. We obtained 25 intermediate models per one homology modeling in MOE, and selected the 3-D model with best total scores according to the generalized Born/volume integral methodology (Labute, 2008). The final 3-D model was thermodynamically optimized by energy minimization using an AMBER12EHT force field (Gerber and Müller, 1995) combined with the generalized Born model of aqueous solvation implemented in MOE (Onufriev et al., 2000). Physically unacceptable local structures of the optimized 3-D models were further refined on the basis of evaluation by the Ramachandran plot using MOE.

Mass spectrometry. Overexpressed RORγt in 293T cells and endogenous RORγt from thymocytes and Th17 cells were prepared identically as for IP of RORγt. In brief, RORγt from 293T cells, was immunoprecipitated from six 10-cm plates pooled per condition, and RORγt from thymocytes and Th17 cells was immunoprecipitated from a pool of 10 WT mice and from a pool 10 Sirt1$^{-/-}$ mice, respectively. In all cases, after IP and after elution of RORγt, samples were run in Laemmli buffer on 4–12% Bis-Tris Criterion XT Gels (Bio-Rad Laboratories) and visualized with Coomassie Blue (SimplyBlue; Invitrogen). Gel bands were excised, destained, reduced with a final concentration of 10 mM dithiothreitol at 56°C, and alkylated with 55 mM iodoacetamide at room temperature in the dark. In-gel trypsin digestion was performed using a 1:20 enzyme to protein ratio overnight at 37°C. Resulting peptides were extracted and desalted. All samples were analyzed by reverse-phase HPLC-ESI-MS/MS using an Eksigent Ultra Plus nano-LC 2D HPLC system connected to either a quadrupole time-of-flight TripleTOF 5600 or 6600 mass spectrometer (AB SCIEX). Typically, mass resolution for MS1 scans and corresponding precursor ions was ∼35,000 (TripleTOF 5600) or ∼48,000 (TripleTOF 6600), whereas resolution for MS2 scans was ∼15,000 ('high sensitivity' product ion scan mode). Samples were acquired by reverse-phase HPLC-ESI-MS/MS using an Eksigent Ultra Plus nano-LC 2D HPLC system which was connected to a quadrupole time-of-flight TripleTOF 5600 mass spectrometer (AB SCIEX, Concord, CAN).

After injection, peptide mixtures were transferred onto the analytical C18-nanocapillary HPLC column (C18 Acclaim PepMap100; 75 μm I.D. × 15 cm, 3 μm particle size, 100 Å pore size; Dionex) and eluted at a flow rate of 300 nl/min using the following gradient: at 5% solvent B in A (from 0–15 min), 5–8% solvent B in A (from 15–18 min), 8–28% solvent B in A (from 18–67 min), 28–80% solvent B in A (from 67–77 min), at 80% solvent B in A (from 77–87 min), with a total runtime of 120 min including mobile phase equilibration. Solvents were prepared as follows, mobile phase A: 2% acetonitrile/98% of 0.1% formic acid (vol/vol) in water, and mobile phase B: 98% acetonitrile/2% of 0.1% formic acid (vol/vol) in water. For overexpressed RORγt detection, (2x biological replicates of p300+RORγt, and p300+RORγt+SIRT1, respectively) data acquisition was performed in the data dependent mode (DDA) on the TripleTOF 5600 to obtain MS/MS spectra for the 30 most abundant precursor ions (∼50 ms per MS/MS) after each survey MS1 scan (250 ms) for a total cycle time of 1.8 s For endogenous

RORγt detection isolated from thymocytes and Th17 cells, data were similarly acquired in a DDA mode; however, we also used MRM-HR data-independent acquisition (DIA) mode (2× technical replicates each). The assay cycled through the entire gradient allowing for one 250 ms MS1 scan followed by 22 MS/MS targeting distinct and predefined precursor ions (acetylated RORγt peptides and some unmodified control peptides), yielding a total cycle time of 2.9 s.

Bioinformatic database searches. Mass spectrometric data were searched using the database search engine ProteinPilot (Shilov et al., 2007; AB SCIEX Beta 4.5, revision 1656) with the Paragon algorithm (4.5.0.0, 1654). The search parameters were set as follows: trypsin digestion, cysteine alkylation set to iodoacetamide, acetylation emphasis, and species *M. musculus*. Trypsin specificity was assumed as C-terminal cleavage at lysine and arginine. Processing parameters were set to "Biological modification" and a thorough ID search effort was used. For database searches, a cut-off peptide confidence value of 99 was chosen. The Protein Pilot false discovery rate (FDR) analysis tool, the Proteomics System Performance Evaluation Pipeline (PSPEP algorithm; Shilov et al., 2007) provided a global FDR of 1% and a local FDR at 1% in all cases. Data were also analyzed using a Mascot (Perkins et al., 1999) server version 2.3.02 after initially generating peak lists with the AB SCIEX mgf data converter version 1.3. All database search results and details for peptide identifications are provided in Table S1.

Quantitative Skyline MS1 filtering and MRM-HR data analysis. MS1 and MS2 chromatogram based quantification was performed in Skyline 2.5 (MacLean et al., 2010) an open source software project as recently described in detail for MS1 Filtering (Schilling et al., 2012). In brief, comprehensive spectral libraries were generated in Skyline from database searches of the raw data files before MS1 Filtering. Next, all raw files acquired in data dependent acquisition mode (DDA), were directly imported into Skyline 2.5 and MS1 precursor ions are extracted for all peptides present in the MS/MS spectral libraries. Quantitative MS1 analysis is based on extracted ion chromatograms (XICs) and resulting precursor ion peak areas for M, M+1, and M+2. Final quantitative comparisons are typically based on only the highest ranked precursor ion, and were exported from Skyline for the various acetyl-lysine peptides examined in the 293T cell experiments. MRM-HR datasets for thymocytes and Th17 cells were also imported into Skyline; however, in this targeted DIA assay, quantification is based on extracted ion chromatograms of MS/MS fragment ions, typically y- and b-ions, matching to specific (acetylated) peptides present in the spectral libraries. Resulting MS2 fragment ion peak areas of highly ranked fragment ions were summed for each peptide and statistically processed to assess differences between WT and Sirt1$^{-/-}$ mice. In all cases, significance was assessed using two-tailed Student's *t* test ($P < 0.05$).

Raw data accession and panorama spectral libraries. The mass spectrometric raw data associated with this manuscript can be downloaded from the Center for Computational Mass Spectrometry under the 'Mass spectrometry Interactive Virtual Environment', MassIVE, ID number. A spectral library with MS/MS spectra for all peptides/proteins used for Skyline MS1 Filtering and MRM-HR data analysis, and subsequent quantification was transferred and published to the interactive, web-based data sharing Panorama portal (Sharma et al., 2014).

Online supplemental material. Fig. S1 shows tandem mass spectra and acetylated lysine residues in RORγt with corresponding MRM-HR data. Protein abundance and acetylation changes of RORγt from WT and Sirt1$^{-/-}$ mice in Th17 cells and thymocytes are shown in Fig. S2 and Fig. S3, respectively. Table S1 shows mass spectrometric identification details of RORγt. Table S2 shows overview and quantification/identification details of RORγt from WT and Sirt1$^{-/-}$ mice observed by MRM-HR. Online supplemental material is available at http://www.jem.org/cgi/content/full/jem.20132378/DC1.

We thank John Carroll, Chris Goodfellow, and Teresa Roberts for figure preparation, and the members of Verdin laboratory for discussion.

This work was supported by the Gladstone Institutes and by generous support from the Kurtzig and Mulholland families to E. Verdin and M. Ott, National Institutes of Health Grant (NIH/NIDA, 1DP1DA038043) to M. Ott, National Institutes of Health grant (R01 NS052189) to K. Akassoglou, NCRR shared instrumentation grant for TripleTOF 6600 (1S10 OD016281) to B.W. Gibson, and R01 NS052189 grant to K. Akassoglou.

E. Verdin was a member of the Scientific Advisory Board of SIRTRIS/GlaxoSmithKline during the course of these studies and until September 30, 2014. The authors have no additional financial interests.

Author contributions: H.W. Lim and E. Verdin conceived and designed the project. H.W. Lim, S.G. Kang, J.RK. Ryu B. Schilling, M. Fei, I.S. Lee, A. Kehasse, H.G. Kasler, H.-S. Kwon, K. Shirakawa, M. Schnölzer, and M. Yokoyama performed experiments. B.W. Gibson, H. Sato, M. Ott, K. Akassoglou, C. Xiao, and E. Verdin supervised the experiments. H.W. Lim, I.S. Lee, H.G. Kasler, D.R. Littman, and E. Verdin participated in manuscript preparation. H.W. Lim, D.R. Littman, and E. Verdin participated in designing experiments. All authors discussed and reviewed the manuscript.

Submitted: 15 November 2013
Accepted: 3 April 2015

REFERENCES

Adams, R.A., J. Bauer, M.J. Flick, S.L. Sikorski, T. Nuriel, H. Lassmann, J.L. Degen, and K. Akassoglou. 2007. The fibrin-derived gamma377-395 peptide inhibits microglia activation and suppresses relapsing paralysis in central nervous system autoimmune disease. *J. Exp. Med.* 204:571–582. http://dx.doi.org/10.1084/jem.20061931

Beier, U.H., L. Wang, T.R. Bhatti, Y. Liu, R. Han, G. Ge, and W.W. Hancock. 2011. Sirtuin-1 targeting promotes Foxp3+ T-regulatory cell function and prolongs allograft survival. *Mol. Cell. Biol.* 31:1022–1029. http://dx.doi.org/10.1128/MCB.01206-10

Davalos, D., J.K. Ryu, M. Merlini, K.M. Baeten, N. Le Moan, M.A. Petersen, T.J. Deerinck, D.S. Smirnoff, C. Bedard, H. Hakozaki, et al. 2012. Fibrinogen-induced perivascular microglial clustering is required for the development of axonal damage in neuroinflammation. *Nat. Commun.* 3:1227. http://dx.doi.org/10.1038/ncomms2230

Gao, B., Q. Kong, K. Kemp, Y.S. Zhao, and D. Fang. 2012. Analysis of sirtuin 1 expression reveals a molecular explanation of IL-2-mediated reversal of T-cell tolerance. *Proc. Natl. Acad. Sci. USA.* 109:899–904. http://dx.doi.org/10.1073/pnas.1118462109

Gerber, P.R., and K. Müller. 1995. MAB, a generally applicable molecular force field for structure modelling in medicinal chemistry. *J. Comput. Aided Mol. Des.* 9:251–268. http://dx.doi.org/10.1007/BF00124456

He, Y.W., M.L. Deftos, E.W. Ojala, and M.J. Bevan. 1998. RORgamma t, a novel isoform of an orphan receptor, negatively regulates Fas ligand expression and IL-2 production in T cells. *Immunity.* 9:797–806. http://dx.doi.org/10.1016/S1074-7613(00)80645-7

Ivanov, I.I., B.S. McKenzie, L. Zhou, C.E. Tadokoro, A. Lepelley, J.J. Lafaille, D.J. Cua, and D.R. Littman. 2006. The orphan nuclear receptor RORgammat directs the differentiation program of proinflammatory IL-17+ T helper cells. *Cell.* 126:1121–1133. http://dx.doi.org/10.1016/j.cell.2006.07.035

Kebir, H., K. Kreymborg, I. Ifergan, A. Dodelet-Devillers, R. Cayrol, M. Bernard, F. Giuliani, N. Arbour, B. Becher, and A. Prat. 2007. Human TH17 lymphocytes promote blood-brain barrier disruption and central nervous system inflammation. *Nat. Med.* 13:1173–1175. http://dx.doi.org/10.1038/nm1651

Kwon, H.S., M.M. Brent, R. Getachew, P. Jayakumar, L.F. Chen, M. Schnolzer, M.W. McBurney, R. Marmorstein, W.C. Greene, and M. Ott. 2008. Human immunodeficiency virus type 1 Tat protein inhibits the SIRT1 deacetylase and induces T cell hyperactivation. *Cell Host Microbe.* 3:158–167. http://dx.doi.org/10.1016/j.chom.2008.02.002

Kwon, H.S., H.W. Lim, J. Wu, M. Schnölzer, E. Verdin, and M. Ott. 2012. Three novel acetylation sites in the Foxp3 transcription factor regulate the suppressive activity of regulatory T cells. *J. Immunol.* 188:2712–2721. http://dx.doi.org/10.4049/jimmunol.1100903

Labute, P. 2008. The generalized Born/volume integral implicit solvent model: estimation of the free energy of hydration using London dispersion

instead of atomic surface area. *J. Comput. Chem.* 29:1693–1698. http://dx.doi.org/10.1002/jcc.20933

Laurence, A., C.M. Tato, T.S. Davidson, Y. Kanno, Z. Chen, Z. Yao, R.B. Blank, F. Meylan, R. Siegel, L. Hennighausen, et al. 2007. Interleukin-2 signaling via STAT5 constrains T helper 17 cell generation. *Immunity.* 26:371–381. http://dx.doi.org/10.1016/j.immuni.2007.02.009

Littman, D.R., Z. Sun, D. Unutmaz, M.J. Sunshine, H.T. Petrie, and Y.R. Zou. 1999. Role of the nuclear hormone receptor ROR gamma in transcriptional regulation, thymocyte survival, and lymphoid organogenesis. *Cold Spring Harb. Symp. Quant. Biol.* 64:373–381. http://dx.doi.org/10.1101/sqb.1999.64.373

MacLean, B., D.M. Tomazela, N. Shulman, M. Chambers, G.L. Finney, B. Frewen, R. Kern, D.L. Tabb, D.C. Liebler, and M.J. MacCoss. 2010. Skyline: an open source document editor for creating and analyzing targeted proteomics experiments. *Bioinformatics.* 26:966–968. http://dx.doi.org/10.1093/bioinformatics/btq054

Onufriev, A., D. Bashford, and D.A. Case. 2000. Modification of the generalized Born model suitable for macromolecules. *J. Phys. Chem. B.* 104:3712–3720. http://dx.doi.org/10.1021/jp994072s

Perkins, D.N., D.J. Pappin, D.M. Creasy, and J.S. Cottrell. 1999. Probability-based protein identification by searching sequence databases using mass spectrometry data. *Electrophoresis.* 20:3551–3567. http://dx.doi.org/10.1002/(SICI)1522-2683(19991201)20:18<3551::AID-ELPS3551>3.0.CO;2-2

Quintana, F.J., H. Jin, E.J. Burns, M. Nadeau, A. Yeste, D. Kumar, M. Rangachari, C. Zhu, S. Xiao, J. Seavitt, et al. 2012. Aiolos promotes TH17 differentiation by directly silencing Il2 expression. *Nat. Immunol.* 13:770–777. http://dx.doi.org/10.1038/ni.2363

Rastinejad, F., T. Perlmann, R.M. Evans, and P.B. Sigler. 1995. Structural determinants of nuclear receptor assembly on DNA direct repeats. *Nature.* 375:203–211. http://dx.doi.org/10.1038/375203a0

Schilling, B., M.J. Rardin, B.X. MacLean, A.M. Zawadzka, B.E. Frewen, M.P. Cusack, D.J. Sorensen, M.S. Bereman, E. Jing, C.C. Wu, et al. 2012. Platform-independent and label-free quantitation of proteomic data using MS1 extracted ion chromatograms in skyline: application to protein acetylation and phosphorylation. *Mol. Cell. Proteomics.* 11:202–214. http://dx.doi.org/10.1074/mcp.M112.017707

Sharma, V., J. Eckels, G.K. Taylor, N.J. Shulman, A.B. Stergachis, S.A. Joyner, P. Yan, J.R. Whiteaker, G.N. Halusa, B. Schilling, et al. 2014. Panorama: a targeted proteomics knowledge base. *J. Proteome Res.* 13:4205–4210. http://dx.doi.org/10.1021/pr5006636

Shilov, I.V., S.L. Seymour, A.A. Patel, A. Loboda, W.H. Tang, S.P. Keating, C.L. Hunter, L.M. Nuwaysir, and D.A. Schaeffer. 2007. The Paragon Algorithm, a next generation search engine that uses sequence temperature values and feature probabilities to identify peptides from tandem mass spectra. *Mol. Cell. Proteomics.* 6:1638–1655. http://dx.doi.org/10.1074/mcp.T600050-MCP200

Shirakawa, K., A. Takaori-Kondo, M. Yokoyama, T. Izumi, M. Matsui, K. Io, T. Sato, H. Sato, and T. Uchiyama. 2008. Phosphorylation of APOBEC3G by protein kinase A regulates its interaction with HIV-1 Vif. *Nat. Struct. Mol. Biol.* 15:1184–1191. http://dx.doi.org/10.1038/nsmb.1497

van Loosdregt, J., Y. Vercoulen, T. Guichelaar, Y.Y. Gent, J.M. Beekman, O. van Beekum, A.B. Brenkman, D.J. Hijnen, T. Mutis, E. Kalkhoven, et al. 2010. Regulation of Treg functionality by acetylation-mediated Foxp3 protein stabilization. *Blood.* 115:965–974. http://dx.doi.org/10.1182/blood-2009-02-207118

Yamane, H., and W.E. Paul. 2012. Cytokines of the γ(c) family control CD4+ T cell differentiation and function. *Nat. Immunol.* 13:1037–1044. http://dx.doi.org/10.1038/ni.2431

Zhang, F., G. Meng, and W. Strober. 2008. Interactions among the transcription factors Runx1, RORgammat and Foxp3 regulate the differentiation of interleukin 17-producing T cells. *Nat. Immunol.* 9:1297–1306. http://dx.doi.org/10.1038/ni.1663

Zhang, J., S.M. Lee, S. Shannon, B. Gao, W. Chen, A. Chen, R. Divekar, M.W. McBurney, H. Braley-Mullen, H. Zaghouani, and D. Fang. 2009. The type III histone deacetylase Sirt1 is essential for maintenance of T cell tolerance in mice. *J. Clin. Invest.* 119:3048–3058. http://dx.doi.org/10.1172/JCI38902

Zhao, Q., S.A. Chasse, S. Devarakonda, M.L. Sierk, B. Ahvazi, and F. Rastinejad. 2000. Structural basis of RXR-DNA interactions. *J. Mol. Biol.* 296:509–520. http://dx.doi.org/10.1006/jmbi.1999.3457